2003

Theoretical Analysis for Obtaining Physical Properties of Composite Electrodes

Parthasarathy M. Gomadam
University of South Carolina - Columbia

John W. Weidner
University of South Carolina - Columbia, weidner@engr.sc.edu

Thomas A. Zawodzinski

Andrew P. Saab

Publication Info

Journal of the Electrochemical Society, 2003, pages E371-E376.

Publisher's link:
http://dx.doi.org/10.1149/1.1586301
DOI: 10.1149/1.1586301

Journal of The Electrochemical Society, **150** (8) E371-E376 (2003)
0013-4651/2003/150(8)/E371/6/$7.00 © The Electrochemical Society, Inc.

Theoretical Analysis for Obtaining Physical Properties of Composite Electrodes

Parthasarathy M. Gomadam,[a,*] John W. Weidner,[a,,z] Thomas A. Zawodzinski,[b,**] and Andrew P. Saab[b,**]**

[a]*Center for Electrochemical Engineering, Department of Chemical Engineering, University of South Carolina, Columbia, South Carolina 29208, USA*
[b]*Los Alamos National Laboratory, Los Alamos, New Mexico 87545, USA*

A theoretical analysis is presented that allows *in situ* measurements of the physical properties of a composite electrode, namely, the electronic conductivity, the ionic conductivity, the exchange-current density, and the double-layer capacitance. Use is made of the current-voltage responses of the composite electrode to dc and ac polarizations under three different experimental configurations. This analysis allows the physical properties to be obtained even when the various resistances in the composite (*e.g.*, ionic, electronic, and charge-transfer) are of comparable values.
 [DOI: 10.1149/1.1586301]

Manuscript submitted July 23, 2002; revised manuscript received February 14, 2003. Available electronically June 23, 2003.

Composite electrodes, composed of a mixture of electronically and ionically conducting materials, are key components in a range of electrochemical devices (*e.g.*, Li-ion batteries and fuel cells). The development of optimum composite electrodes for a particular application is hampered by a lack of understanding of how cell assembly, processing conditions, additives (*e.g.*, binders, surfactants), and operation affect the performance of the electrode. Therefore, *in situ* measurements are needed to correlate changes in the electrode to its physical properties. For example, Shibuya *et al.*[1] investigated the electronic conductivity of a composite cathode in a lithium battery, and Saab *et al.*[2] the ionic and electronic conductivities of Nafion/carbon composites. Shibuya *et al.*[1] used an interdigitated array of electrodes to measure the electronic conductivity of Li_xCoO_2 while simultaneously intercalating (or deintercalating) lithium into it. In their analysis, the measured current, *I*, that flowed between the adjacent electrodes in the array and the potential difference, *V*, that was applied between them, were used to obtain the electronic conductance of the composite electrode from Ohm's law

$$\sigma = \frac{IL}{V} \qquad [1]$$

where *L* was the distance between the two electrodes. The application of Eq. 1 to composite electrodes assumes that there is no interaction between the ionic and electronic phases. In other words, charge-transfer or ionic resistance must be the dominant resistance for σ to be determined from a single data point. For situations when this condition does not hold, the technique used by Shibuya *et al.*[1] would yield only a combination of ionic, electronic, and charge-transfer resistances, not just the electronic resistance of the solid phase. In order to decouple the various resistances, a more complete set of data (*e.g.*, different experimental configurations, full impedance spectrum) must be analyzed to accurately determine the ionic, electronic, and charge-transfer resistances.

In this work, we examine three different configurations of operation of the composite and analyze their dynamic response under conditions of dc and ac polarization. The results confirm that one resistance can be obtained from a single data point only when the other resistances dominate. When the various resistances are comparable, we provide a method to decouple the various resistances from sets of experimental dc or ac polarization data.

Theory

The three configurations considered are shown schematically in Fig. 1. The shaded region denotes the composite electrode of thickness *L*, composed of a mixture of ionically and electronically conducting phases. In configuration I, the reference electrode is placed in the electrolyte at a point near the face of the composite working electrode (*i.e.*, at $x = 0$) and the other side of the composite is supported by a metallic current collector (*i.e.*, at $x = L$). In configuration II, the composite is bound by current collectors on either side, while in configuration III, it is bound by two reference electrodes. In all three configurations, a current, *I*, flows between points A and B, while the resulting potential difference, *V*, is measured between points C and D. Configurations II and III, respectively, represent the conventional two- and four-probe conductivity methods.

The following analysis (dc and ac) applies porous electrode theory, which treats the composite electrode as a superposition of two continua or phases.[3] One phase represents a purely ionically

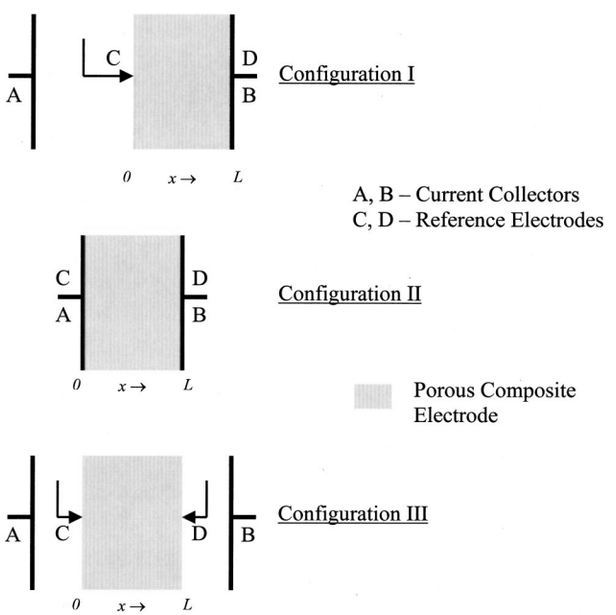

Figure 1. Schematic of a composite electrode under three different configurations labeled I, II, and III. The electrolyte fills the unshaded area between the current collectors as well as the pores in the composite. In all three configurations, current flows between points A and B, while the resulting potential difference is measured between points C and D.

* Electrochemical Society Student Member.
** Electrochemical Society Active Member.
z E-mail: weidner@engr.sc.edu

conducting solution and the other a purely electronically conducting solid. The dc analysis is applicable for those times after a small step change in either the current or the potential difference, when concentration variations are negligible. Thus, in the steady-state regions discussed in this paper, the times are not long enough for any appreciable mass-transfer effect to occur. Similarly, the ac analysis applies for those frequencies, when concentration variation are negligible. Thus, in the low-frequency regions discussed in this paper, the frequencies are not low enough for any appreciable mass-transfer effect to occur. Further, invariant physical properties, namely, the solid-phase electronic conductivity σ, the solution phase ionic conductivity κ, the interfacial exchange-current density i_0, and the double-layer capacitance C, are assumed. Additional assumptions are noted where appropriate.

For all three configurations, Ohm's law applies in each phase of the composite electrode, giving

$$i_1 = -\sigma \frac{d\phi_1}{dx} \quad [2]$$

and

$$i_2 = -\kappa \frac{d\phi_2}{dx} \quad [3]$$

Further, the application of charge balance inside the electrode leads to the following relationships[3]

$$\sigma \frac{\partial^2 \phi_1}{\partial x^2} = aC \frac{\partial(\phi_1 - \phi_2)}{\partial t} + ai_0 nf(\phi_1 - \phi_2) \quad [4]$$

and

$$\kappa \frac{\partial^2 \phi_2}{\partial x^2} = -aC \frac{\partial(\phi_1 - \phi_2)}{\partial t} - ai_0 nf(\phi_1 - \phi_2) \quad [5]$$

The first term on the right side of Eq. 4 and 5 is due to double-layer charging and the second term is the linearized form of the kinetic expression for the faradaic reaction. Therefore, this analysis holds for small perturbations in the current or potential.

Eqs. 4 and 5 form the governing equations for the potential in all three configurations. However, the three configurations differ in the boundary conditions depending on which phase carries current at the boundaries. In configuration I, all the current is carried by the ionic phase at $x = 0$ and by the electronic phase at $x = L$, leading to

$$\begin{aligned} &\text{at} \quad x = 0, \; i_1 = 0 \;\text{ and }\; i_2 = I \\ &\text{at} \quad x = L, \; i_1 = I \;\text{ and }\; i_2 = 0 \end{aligned} \quad [6]$$

In configuration II, all the current is carried by the electronic phase at both boundaries, leading to

$$\begin{aligned} &\text{at} \quad x = 0, \; i_1 = I \;\text{ and }\; i_2 = 0 \\ &\text{at} \quad x = L, \; i_1 = I \;\text{ and }\; i_2 = 0 \end{aligned} \quad [7]$$

while in configuration III, all the current is carried by the ionic phase at both boundaries, leading to

$$\begin{aligned} &\text{at} \quad x = 0, \; i_1 = 0 \;\text{ and }\; i_2 = I \\ &\text{at} \quad x = L, \; i_1 = 0 \;\text{ and }\; i_2 = I \end{aligned} \quad [8]$$

The initial condition for all the three configurations is set as

$$\phi_1 - \phi_2 = 0 \quad [9]$$

DC response.—Equations 2-9 are solved analytically by the method of separation of variables[4] to obtain the transient potential drops, V^k, between points C and D (see Fig. 1) in the three configurations, following a small step change in the applied current. These solutions are identical to those of the transient currents following a small step change in the applied potentials. Therefore, the solutions are expressed as dimensionless resistances, $R^k \equiv \sigma V^k / I^k L$, which are

$$R^k = R^k_\infty + R_\Omega \sum_{m=0}^{\infty} C^k_m e^{-(m^2\pi^2 + \nu^2)\tau} \quad [10]$$

where

$$C^k_m = 2\frac{[(-1)^m - (2 + \kappa/\sigma)]}{(m^2\pi^2 + \nu^2)}[A^k \sinh\nu + B^k \cosh\nu - B^k(-1)^m] \quad [11]$$

except C^k_0 is half the value calculated from Eq. [11], and

$$R_\Omega = \frac{1}{1 + (\kappa/\sigma)} \quad [12]$$

$$\nu = L\sqrt{\frac{a(\kappa + \sigma)}{\kappa\sigma}(i_0 nf)} \quad [13]$$

$$\tau = \frac{t}{\frac{L^2 aC}{\sigma}\left(1 + \frac{1}{\kappa/\sigma}\right)} \quad [14]$$

$$A^I = -\frac{1}{(\kappa/\sigma)}\left[\frac{(\kappa/\sigma) + \cosh\nu}{\nu \sinh\nu}\right] \quad B^I = \frac{1}{(\kappa/\sigma)\nu} \quad [15]$$

$$A^{II} = -\left(\frac{1 - \cosh\nu}{\nu \sinh\nu}\right) \quad B^{II} = -\frac{1}{\nu} \quad [16]$$

$$A^{III} = \frac{1}{(\kappa/\sigma)}\left(\frac{1 - \cosh\nu}{\nu \sinh\nu}\right) \quad B^{III} = \frac{1}{(\kappa/\sigma)\nu} \quad [17]$$

The steady-state dimensionless resistances, R^k_∞, are given by

$$R^I_\infty = R_\Omega\left[1 + \frac{2 + \left(\frac{\sigma}{\kappa} + \frac{\kappa}{\sigma}\right)\cosh\nu}{\nu \sinh\nu}\right] \quad [18]$$

$$R^{II}_\infty = R_\Omega\left[1 - 2\left(\frac{\kappa}{\sigma}\right)\left(\frac{1 - \cosh\nu}{\nu \sinh\nu}\right)\right] \quad [19]$$

$$R^{III}_\infty = R_\Omega\left[1 - 2\left(\frac{\sigma}{\kappa}\right)\left(\frac{1 - \cosh\nu}{\nu \sinh\nu}\right)\right] \quad [20]$$

for the three configurations, respectively. Newman[3] and Ong and Newman[5] present analytical solutions for the steady-state and transient resistances for configuration I. The solutions for configuration I have been repeatedly used by numerous researchers and are presented here for the sake of continuity.

For short times, Eq. 10 is linearized and a plot of R^k *vs.* τ yields a straight line. Following Ong and Newman,[5] a dimensionless short-

time time-intercept (τ_C^k) is defined as that point on the τ-axis where the short-time straight line R^k *vs.* τ intersects R_∞^k. For the three configurations, this intercept is given by

$$\tau_C^k = \frac{\sum_{m=0}^{\infty} C_m^k}{\sum_{m=0}^{\infty} C_m^k (m^2\pi^2 + \nu^2)} \quad [21]$$

AC response.—In order to obtain the frequency responses of the three configurations, Eq. 4 and 5 are transformed from the time domain (t) into the Laplace domain (s) to give

$$\sigma \frac{\partial^2 \bar{\phi}_1}{\partial x^2} = aCs(\bar{\phi}_1 - \bar{\phi}_2) + ai_0 nf(\bar{\phi}_1 - \bar{\phi}_2) \quad [22]$$

and

$$\kappa \frac{\partial^2 \bar{\phi}_2}{\partial x^2} = -aCs(\bar{\phi}_1 - \bar{\phi}_2) - ai_0 nf(\bar{\phi}_1 - \bar{\phi}_2) \quad [23]$$

Equations 22 and 23 are similar to the steady-state forms of Eq. 4 and 5. Further, after substituting $s = j\omega$ and defining ν_{AC} as

$$\nu_{AC} = L\sqrt{\frac{a(\kappa + \sigma)}{\kappa\sigma}(i_0 nf + C\omega j)} \quad [24]$$

the governing equations and boundary conditions for ac polarization in the frequency domain are identical to those of dc polarization at steady state. Consequently, Eq. 18-20 give the dimensionless impedance (Z^k) in the corresponding configurations, with ν_{AC} of Eq. 24 used in place of ν. Thus, the dimensionless impedances are given by

$$Z^I = R_\Omega\left[1 + \frac{2 + \left(\frac{\sigma}{\kappa} + \frac{\kappa}{\sigma}\right)\cosh\nu_{AC}}{\nu_{AC}\sinh\nu_{AC}}\right] \quad [25]$$

$$Z^{II} = R_\Omega\left[1 - 2\left(\frac{\kappa}{\sigma}\right)\left(\frac{1 - \cosh\nu_{AC}}{\nu_{AC}\sinh\nu_{AC}}\right)\right] \quad [26]$$

$$Z^{III} = R_\Omega\left[1 - 2\left(\frac{\sigma}{\kappa}\right)\left(\frac{1 - \cosh\nu_{AC}}{\nu_{AC}\sinh\nu_{AC}}\right)\right] \quad [27]$$

for the three configurations, respectively. Since j occurs under the square root in ν_{AC}, the separation of the impedances into real and imaginary parts results in lengthy expressions and are therefore not given here. However, a variety of commercial softwares (*e.g.*, Matlab and Maple) can be used to separate the real and imaginary parts easily. In this work, we used Matlab to evaluate and plot the real and imaginary parts for a range of frequencies to obtain Nyquist impedance spectra.

For all the configurations at low frequencies (*i.e.*, as $\omega \to 0$), ν_{AC} approaches ν, and consequently, Z^k approaches R_∞^k. For all the configurations at high frequencies, the real and imaginary parts of the impedances differ only by R_Ω (*i.e.*, $Z_i^k = R_\Omega - Z_r^k$ and $-dZ_i^k/dZ_r^k = 1$), with the real components given by

$$Z_r^I = \left[1 + \frac{4}{b^3}e^{-4b}\left(\frac{\kappa}{\sigma} + \frac{\sigma}{\kappa}\right)\right]R_\Omega \quad [28]$$

$$Z_r^{II} = \left[1 + \frac{4}{b(\kappa/\sigma)}\tanh(b)\right]R_\Omega \quad [29]$$

$$Z_r^{III} = \left[1 + \frac{4(\kappa/\sigma)}{b}\tanh(b)\right]R_\Omega \quad [30]$$

where

$$b = L\sqrt{\frac{aC\omega(\kappa + \sigma)}{2\kappa\sigma}} \quad [31]$$

Further, as $\omega \to \infty$, the terms inside the square brackets in Eq. 28-30 tend to unity, and Z_r^k and Z_i^k approach R_Ω and 0, respectively.

Impedance models have been developed by Meyers *et al.*,[6] Doyle *et al.*,[7] and Guo *et al.*[8] for a Li-ion battery, and by Srinivasan and Weidner[9] and Motupally *et al.*[10] for the capacitive response of an electrochemical system. Meyers *et al.*[6] included lithium diffusion inside the solid electrode particles and derived analytical solutions for the impedance response of a porous electrode. Doyle *et al.*[7] and Guo *et al.*[8] numerically evaluated the impedance response of a Li-ion battery considering mass-transfer limitations in both solid and solution phases. Srinivasan and Weidner[9] developed analytical solutions for both constant current and impedance responses of an electrochemical capacitor while Motupally *et al.*[10] modeled the capacitive response due to H^+ diffusion through NiOOH. However, the configurations considered by these authors correspond only to configuration I of this study.

Results and Discussion

Figure 2 shows the dimensionless transient dc resistance of the composite for the three configurations simulated using Eq. 10, with $\kappa/\sigma = 1.25$ and $\nu = 10$. At $\tau = 0$, the double-layer capacitance short circuits, resulting in negligible charge transfer across the interface, and consequently, $R^k = R_\Omega$. As τ increases, the impedance due to double-layer capacitance increases and a greater fraction of the current goes to charge transfer, resulting in a time-varying dc resistance. At long times, the double-layer capacitance tends to open circuit and $R^k \to R_\infty^k$. This steady-state resistance depends on κ/σ and ν, as indicated by Eq. 18-20. However, the qualitative shapes of the transient resistances are independent of these parameters.

Figure 3a shows Nyquist plots of the composite for the three configurations simulated using Eq. 25-27, with $\kappa/\sigma = 1.25$ and $\nu = 10$. In each of the three configurations, the Nyquist plots are characterized by a high-frequency real intercept equal to R_Ω, a high-frequency straight line of unit slope (see Eq. 28-30 for the real components in this region), and a low-frequency real intercept equal to R_∞^k. As mentioned in the dc case, the value of the low-frequency

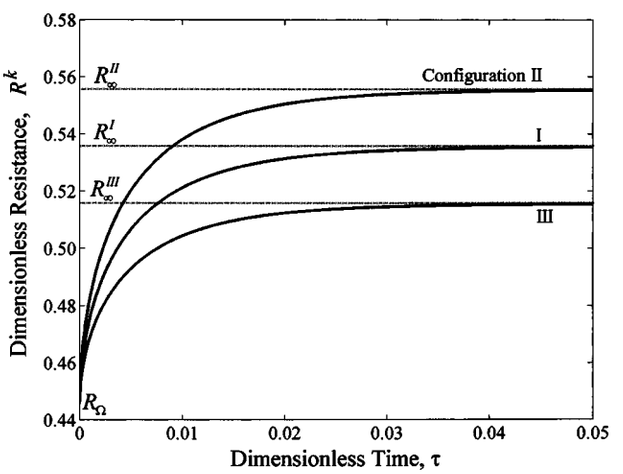

Figure 2. Dimensionless transient resistance of the composite in the three configurations simulated using Eq. 10, with $\kappa/\sigma = 1.25$ and $\nu = 10$. At the instant the circuit is closed, the dimensionless resistances are equal to R_Ω, which is the same as the high-frequency real intercept in the Nyquist plot shown in Fig. 3. The long-time asymptotes, R_∞^k, are the same as the low-frequency intercepts in the Nyquist plot of Fig. 3.

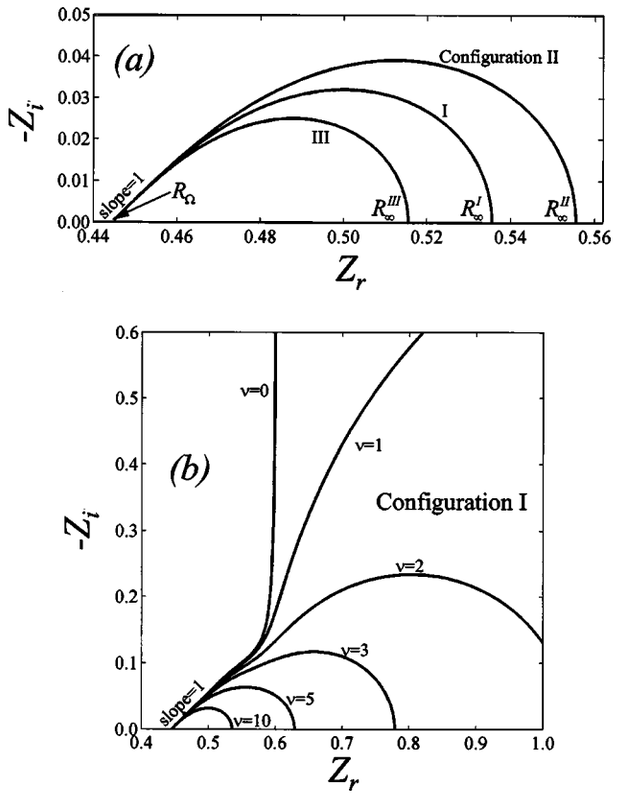

Figure 3. (a) Nyquist plots for the three configurations simulated using Eq. 25-27, with $\kappa/\sigma = 1.25$ and $\nu = 10$. All the curves are characterized by a high-frequency straight line of slope 1 that tends to $(R_\Omega,0)$ as $\omega \to \infty$, and a low-frequency intercept equal to R_∞^k. The high-frequency real intercept (R_Ω) and the low-frequency intercepts (R_∞^k) are the same as the dc resistances at $\tau = 0$ and $\tau \to \infty$, respectively, shown in Fig. 2. (b) Nyquist plots for configuration I as a function of ν for $\kappa/\sigma = 1.25$. Configurations II and III have the same qualitative shape as shown in a, but configuration I tends to infinity as $\nu \to 0$.

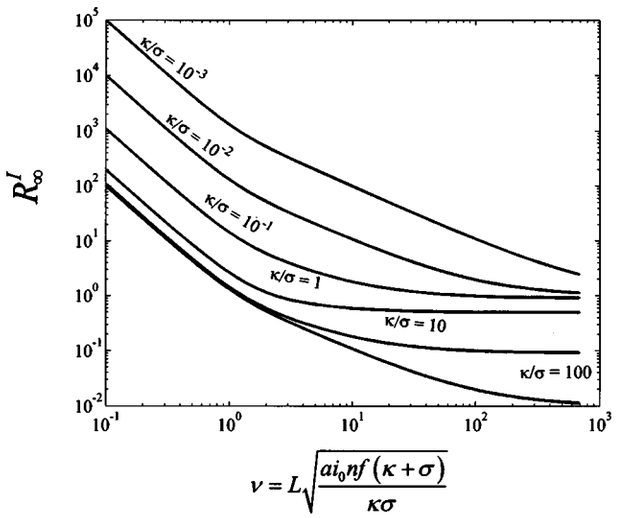

Figure 4. R_∞^I plotted *vs.* ν for different values of (κ/σ). The ordinate is the ratio of the total resistance of the composite to its electronic resistance, for configuration I. R_∞^I asymptotes to R_Ω as $\nu \to \infty$.

intercept (*i.e.*, R_∞^k) is a function of κ/σ and ν. In addition, the qualitative shapes of the Nyquist plots of configurations II and III do not change with ν.

In contrast, Fig. 3b shows that the shape of the Nyquist plot of configuration I varies significantly with ν. The real intercept, R_∞^I, approaches infinity as $\nu \to 0$. At $\nu = 0$, the Nyquist plot does not come back toward the real axis at all. Rather, it behaves as a purely capacitive system, whose impedance tends to infinity as shown by Srinivasan and Weidner[9] and Motupally *et al.*[10]

Two key features of Fig. 2 and 3 are the two limits R_Ω and R_∞^k. R_Ω is a function of one dimensionless parameter, κ/σ, while R_∞^k is a function of two dimensionless parameters, ν and (κ/σ). The parameter ν, as defined in Eq. 13, is the ratio of the ohmic resistance of the composite electrode to its charge-transfer resistance. The dependence of the total steady-state (or low-frequency) resistance of the composite electrode, R_∞^k, on ν and (κ/σ), and the validity of Eq. 1 in determining the charge-transport properties are discussed in the following paragraphs for the three configurations.

Configuration I.—Figure 4 shows the dimensionless resistance R_∞^I (see Eq. 18) plotted *vs.* ν for different values of (κ/σ). The ordinate in Fig. 4 is the ratio of the total resistance of the composite to its electronic resistance. When ionic resistance dominates $(\kappa/\sigma \to 0$ and $\nu \to \infty)$, the current completely bypasses the ionic phase and the total resistance of the composite electrode is equal to its electronic resistance (*i.e.*, $R_\infty^I \to 1$). However, for many practical situations, this criterion is not met. For example, the total resistance in the case of hydrogen oxidation on a Nafion/Pt-carbon composite should be dominated by ionic resistance because of the fast charge-transfer kinetics on Pt and the high electronic conductivity of the composite. Using parameters given by Saab *et al.*[2] ($\kappa = 1$ S/m and $\sigma = 6.25$ S/m) and by Springer *et al.*[11] ($L = 5$ μm and $ai_0 = 8 \times 10^9$ A/m^3), $\kappa/\sigma = 0.16$ and $\nu = 3$. Therefore, from Fig. 4 (or Eq. 18) $R_\infty^I \approx 3$, which means that IL/V_∞^I underpredicts σ by about a factor of 3.0.

For even slower reactions, ν is smaller and the total resistance is even larger than the electronic resistance. In the limit when kinetic resistance dominates (*i.e.*, $\nu \to 0$), $R_\infty^I \to \infty$, as seen in Fig. 4. However, taking the limit of Eq. 18 as $\nu \to 0$ and rewriting it in dimensional form gives $I/V_\infty^I = Lai_0nf$. That is, the reaction rate distribution inside the composite is uniform and i_0 can be determined directly.[3] Thus, when ν is very small kinetic resistance dominates, and when ν is very large ohmic resistance dominates. In other words, the quantity IL/V_∞^I gives, respectively, either $(\kappa + \sigma)$ or i_0. For intermediate values of ν, the current-voltage response is influenced by both kinetic and ohmic resistances and all three parameters must be determined simultaneously.

Configuration II.—As mentioned before, it has been proposed by Shibuya *et al.*,[1] and in Ref. 12-14, that configuration II can be used to estimate the electronic conductivity σ via Eq. 1. In other words, they assumed that the right side of Eq. 19 is equal to unity for all values of (κ/σ) and ν. This assumption, however, holds only when ionic or charge-transfer resistance dominates. Figure 5 shows the dimensionless resistance R_∞^{II} plotted *vs.* ν for different values of (κ/σ). The ordinate in Fig. 5 is the ratio of the total resistance of the composite to its electronic resistance. When charge-transfer resistance is large relative to ohmic resistance (*i.e.*, $\nu \to 0$) R_∞^{II} approaches unity, and therefore, the total resistance of the composite is equal to its electronic resistance. However, as ν increases, the total resistance of the composite is a combination of its ionic, electronic, and kinetic resistances. As $\nu \to \infty$, the total resistance of the composite is equal to its ohmic resistance since R_∞^{II} asymptotes to R_Ω. For the hydrogen oxidation example considered in the previous section (*i.e.*, with $\kappa/\sigma = 0.16$ and $\nu \approx 3$) R_∞^{II} is close to unity, as can be seen from Fig. 5 or Eq. 19. However, in the case of Shibuya *et al.*[1] ($L = 10$ μm, $\sigma \approx 10^{-4}$ S/m from Fig. 2 of Ref. 1) and using the parameters given by Doyle *et al.*[7] ($a = 10^6$ m^{-1}, $i_0 = 1$ A/m^2,

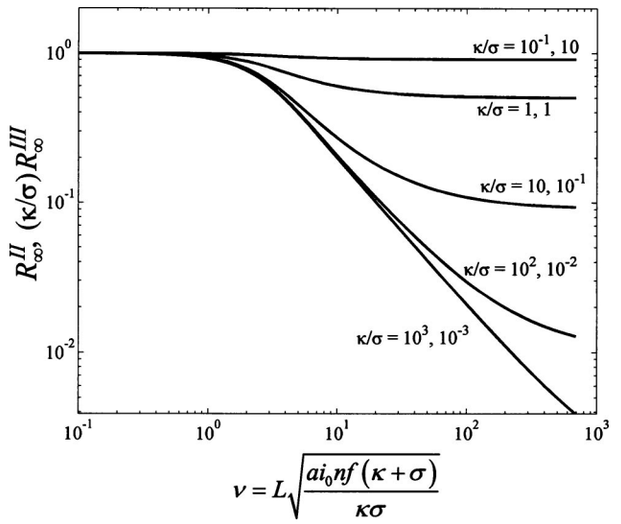

Figure 5. R_∞^{II} [or $(\kappa/\sigma)R_\infty^{III}$] is plotted *vs.* ν for different values of (κ/σ). The ordinate is the ratio of the total resistance of the composite in configuration II (or III) to its electronic (or ionic) resistance. When charge-transfer resistance is low, *i.e.*, when $\nu \to \infty$, R_∞^{II} [or $(\kappa/\sigma)R_\infty^{III}$] asymptotes to R_Ω [or $(\kappa/\sigma)R_\Omega$], while as $\nu \to 0$ it asymptotes to unity.

$\kappa = 0.5$ S/m) we get $\kappa/\sigma = 5000$ and $\nu \approx 6$. Therefore, from Fig. 5 (or Eq. 19) $R_\infty^{II} \approx 0.33$, which means that IL/V_∞^{II} overpredicts the electronic conductivity of $LiCoO_2$ by about a factor of 3.0.

Configuration III.—Analogous to configuration II, Fig. 5 also shows R_∞^{III} (κ/σ) as a function of ν for different values of (κ/σ). The ordinate, in this case, is the ratio of the total resistance of the composite to its ionic resistance. As in configuration II, when charge-transfer resistance becomes very small (*i.e.*, $\nu \to \infty$) R_∞^{III} (κ/σ) asymptotes to R_Ω (κ/σ), and as $\nu \to 0$, R_∞^{III} (κ/σ) asymptotes to unity. In other words, in configuration III the ratio IL/V_∞^{III} gives the ionic conductivity when charge-transfer resistance dominates. For the case of Shibuya *et al.*[1] (*i.e.*, $\kappa/\sigma = 5000$ and $\nu \approx 6$) Fig. 5 or Eq. 20 gives a value for R_∞^{III} (κ/σ) close to unity. However, for the hydrogen oxidation case (*i.e.*, $\kappa/\sigma = 0.16$ and $\nu \approx 3$) R_∞^{III} (κ/σ) $\approx$ 0.66, which means that IL/V_∞^{III} overpredicts the ionic conductivity by about a factor of 1.5.

Parameter estimation.—In the previous section, it was shown that except for some limiting conditions the dc resistance or the ac impedance of a composite electrode is a combination of σ, κ, i_0, and C. Therefore, these parameters must be obtained from a set of data rather than a single data point. For example, these parameters can be obtained by fitting the analytical expressions derived here to the entire ac impedance spectrum or to the entire transient dc resistance, measured on any one of the configurations. Which configuration is chosen depends on how sensitive its response is to the parameter of interest. When the effect of one unknown parameter on the impedance (or transient resistance) of a configuration is much greater than another parameter, then that configuration cannot be used to determine the latter parameter with confidence. One has to use alternative configurations, wherein the response is dominated by the parameter of interest. Since one often does not know the relative importance of the parameters *a priori*, it is prudent to determine the parameters from the responses of multiple configurations. Such use of multiple configurations to determine different parameters has been taken up by Saab *et al.*[2] and Shibuya *et al.*[1]

To complement the parameter estimation using the entire ac impedance spectrum (or the entire transient dc resistance), the limits and intercepts at high and low frequencies (or short and long times) can be used. Further, the limits and intercepts provide quick and valuable insight into the interaction between the parameters. In the following lines, we apply the analysis presented in this paper to describe the estimation of parameters using experimental information on only the limits and intercepts obtained from the three configurations. Here, the dc experiments are treated as taking an applied current as the input and giving a voltage as the response. However, the same analysis is applicable when voltage is taken as the input and current as the response. The following intercepts and limits are used to extract the parameters:

(*i*) The high-frequency intercept obtained from ac impedance, or the initial voltage following a step change in the applied dc current.

(*ii*) The low-frequency intercept obtained from ac impedance, or the steady-state voltage following a step change in the applied dc current.

(*iii*) The frequency dependence of the impedance at high frequencies (*i.e.*, the straight-line portion of the Nyquist curve) obtained from ac impedance, or the short-time time-intercept (τ_C^k) of the voltage following a step change in the applied dc current.

The intercept described in item (*i*), obtained from any of the three configurations, yields the same information: a combination of κ and σ, as also seen from Eq. 12 and Fig. 2 and 3. Thus, by measuring the voltage response at the instant of stepping the current in the case of dc or at high frequencies in the case of ac gives the quantity $\kappa + \sigma$, in all three configurations. The intercepts described in item (*ii*) obtained from the three configurations yield three different combinations of κ, σ, and i_0, as also seen from Eq. 18-20 and Fig. 2 and 3. Thus, information from the intercept in item (*i*) obtained from any one of the configurations (*i.e.*, Eq. 12), and from the intercepts in item (*ii*) obtained from any two of the configurations (*i.e.*, any two of Eq. 18-20) can be used to determine the three unknowns κ, σ, and i_0. With the knowledge of κ, σ, and i_0, the double-layer capacitance (C) could be determined by applying the limiting expression in item (*iii*) to data from any one of the configurations, as also seen from Eq. 21. Tiedemann and Newman[15] have used the short-time response of configuration I in determining the double-layer capacitances of porous Pb and PbO_2 electrodes in H_2SO_4.

Conclusion

The behavior of a porous composite electrode under three different configurations is analyzed for determining the physical properties σ, κ, i_0, and C. Porous electrode theory is used to obtain analytical solutions to the current-voltage response of the three configurations to dc and ac perturbations. These solutions can be used in conjunction with experimental data on either the entire ac impedance spectra or the entire transient dc resistances to obtain the four physical properties. To complement the parameter estimation using the entire ac impedance spectra (or the entire transient dc resistances), the limits and intercepts derived here for high and low frequencies (or for short and long times) can be used. These limiting cases show that in configuration I, the ratio IL/V_∞^I gives either $(\kappa + \sigma)$ when ν is large and i_0 when ν is small. For intermediate values of ν, IL/V_∞^I gives only a combination of σ, κ, and i_0. Similarly, in configuration II (or III), IL/V_∞^{II} (or IL/V_∞^{III}) gives σ (or κ) only when $\sigma \gg \kappa$ (or $\kappa \gg \sigma$), or when ν is small. When these conditions are not valid, one must combine data obtained from dc or ac polarization experiments, conducted on more than one of the three configurations, to evaluate the physical properties. In addition to σ, κ, and i_0, the analysis allows determination of the double-layer capacitance (C) from either short-time dc polarization or high-frequency ac polarization data.

Acknowledgment

The authors acknowledge Dr. Venkat R. Subramanian, Department of Chemical Engineering, University of South Carolina, for his assistance in obtaining some of the analytical solutions presented in this work. This work was supported by the Chemical and Biological Nonproliferation Program of the U.S. Department of Energy.

The University of South Carolina assisted in meeting the publication costs of this article.

List of Symbols

a specific surface area, m^{-1}
b dimensionless quantity as defined in Eq. 31
A^k coefficient, as defined in Eq. 15–17
B^k coefficient, as defined in Eq. 15–17
C double-layer capacitance, F/m^2
C_m coefficient, as defined in Eq. 11
f F/RT, 38.944 V^{-1}
F Faraday's constant, 96,487 C/equiv
i_1 electronic current density, A/m^2
i_2 ionic current density, A/m^2
i_0 exchange current density, A/m^2
I^k total current density for configuration k, A/m^2
j $\sqrt{-1}$
L thickness of the composite electrode, m
n number of electron transfers in the reaction, equiv/mol
$\overline{P}$ any variable P in Laplace domain
R gas constant, 8.314 J/mol/K
R^k dimensionless resistance for configuration k, $\sigma V^k/I^k L$
R_Ω dimensionless resistance, $1/[1 + (\kappa/\sigma)]$
s Laplace domain variable, s^{-1}
t time, s
T temperature, K
V^k voltage for configuration k, V
x space coordinate, m
Z^k dimensionless impedance for configuration k
Z_i^k imaginary part of Z^k
Z_r^k real part of Z^k

Greek

ϕ_1 potential in the electronic phase, V
ϕ_2 potential in the ionic phase, V
κ ionic conductivity of the composite, $\Omega^{-1}\ m^{-1}$
σ electronic conductivity of the composite, $\Omega^{-1}\ m^{-1}$
ν, ν_{AC} dimensionless parameters (see Eq. 13 and 24)
τ dimensionless time, as defined in Eq. 14
τ_C dimensionless short-time time-intercept, as defined in Eq. 21
ω frequency, s^{-1}

Superscript

k configuration k, where k = I, II, or III

Subscript

∞ steady state or low-frequency limit

References

1. M. Shibuya, T. Nishina, T. Matsue, and I. Uchida, *J. Electrochem. Soc.*, **143**, 3157 (1996).
2. A. P. Saab, F. H. Garzon, and T. A. Zawodzinski, *J. Electrochem. Soc.*, **149**, A1541 (2002).
3. J. Newman, *Electrochemical Systems*, Prentice Hall, Inc., Englewood Cliffs, NJ (1991).
4. V. R. Subramanian and R. E. White, *J. Power Sources*, **96**, 385 (2001).
5. I. J. Ong and J. Newman, *J. Electrochem. Soc.*, **146**, 4360 (1999).
6. J. P. Meyers, M. Doyle, R. M. Darling, and J. Newman, *J. Electrochem. Soc.*, **147**, 2930 (2000).
7. M. Doyle, J. P. Meyers, and J. Newman, *J. Electrochem. Soc.*, **147**, 99 (2000).
8. Q. Guo, V. R. Subramanian, J. W. Weidner, and R. E. White, *J. Electrochem. Soc.*, **149**, A307 (2002).
9. V. Srinivasan and J. W. Weidner, *J. Electrochem. Soc.*, **146**, 1650 (1999).
10. S. Motupally, C. C. Streinz, and J. W. Weidner, *J. Electrochem. Soc.*, **142**, 1401 (1995).
11. T. E. Springer, T. Rockward, T. A. Zawodzinski, and S. Gottesfeld, *J. Electrochem. Soc.*, **148**, A11 (2001).
12. M. Shibuya, S. Yamamura, T. Matsue, and I. Uchida, *Chem. Lett.*, **1995**, 749.
13. M. Nishizawa, H. Koshika, and I. Uchida, *J. Phys. Chem.*, **103**, 192 (1999).
14. M. Nishizawa and I. Uchida, *Electrochim. Acta*, **44**, 3629 (1999).
15. W. Tiedemann and J. Newman, *J. Electrochem. Soc.*, **122**, 70 (1975).